Search for tZ' associated production induced by tcZ' couplings at the LHC

Wei-Shu Hou, Masaya Kohda, and Tanmoy Modak
Department of Physics, National Taiwan University, Taipei 10617, Taiwan
(Received 27 February 2017; published 28 July 2017)

The P_5' and R_K anomalies, recently observed by the LHCb Collaboration in $B \to K^{(*)}$ transitions, may indicate the existence of a new Z' boson, which may arise from gauged $L_\mu - L_\tau$ symmetry. Flavor-changing neutral current Z' couplings, such as tcZ', can be induced by the presence of extra vector-like quarks. In this paper we study the LHC signatures of the induced right-handed tcZ' coupling that is inspired by, but not directly linked to, the $B \to K^{(*)}$ anomalies. The specific processes studied are $cg \to tZ'$ and its conjugate process, each followed by $Z' \to \mu^+\mu^-$. By constructing an effective theory for the tcZ' coupling, we first explore in a model-independent way the discovery potential of such a Z' at the 14 TeV LHC with 300 and 3000 fb^{-1} integrated luminosities. We then reinterpret the model-independent results within the gauged $L_\mu - L_\tau$ model. In connection with tcZ', the model also implies the existence of a flavor-conserving ccZ' coupling, which can drive the $c\bar{c} \to Z' \to \mu^+\mu^-$ process. Our study shows that existing LHC results for dimuon resonance searches already constrain the ccZ' coupling, and that the Z' can be discovered in either or both of the $cg \to tZ'$ and $c\bar{c} \to Z'$ processes. We further discuss the sensitivity to the left-handed tcZ' coupling and find that the coupling values favored by the $B \to K^{(*)}$ anomalies lie slightly below the LHC discovery reach even with 3000 fb^{-1}.

DOI: 10.1103/PhysRevD.96.015037

I. INTRODUCTION

Recent measurements performed by the LHCb experiment [1–3] exhibit anomalous $B \to K^{(*)}$ transitions. One is the measurement [1,2] of angular observables for the $B^0 \to K^{*0}\mu^+\mu^-$ decay, which shows a discrepancy from the Standard Model (SM) prediction at the 3.4σ level, mainly driven by the P_5' observable. In another measurement [3] of $B^+ \to K^+\ell^+\ell^-$ decays ($\ell = e$ or μ), LHCb found a further hint for lepton flavor universality violation, namely a 2.6σ deviation of the observable $R_K \equiv \mathcal{B}(B^+ \to K^+\mu^+\mu^-)/\mathcal{B}(B^+ \to K^+e^+e^-)$ from its SM value. These LHCb results are supported by a recent Belle analysis [4], where the angular observables were separately measured for the muon and electron modes of $B \to K^*\ell^+\ell^-$ decays, and the muonic P_5' was found to show the largest discrepancy (at the 2.6σ level) from the SM prediction. Although these anomalies can well be due to statistical fluctuations and/or hadronic uncertainties, it is interesting to investigate whether they can be attributed to physics beyond the SM (BSM). Model-independent analyses by various groups have found that a BSM contribution to the Wilson coefficient C_9^μ, associated with the effective operator $O_9^\mu = (\bar{s}_L\gamma^\alpha b_L)(\bar{\mu}\gamma_\alpha\mu)$, can explain both the P_5' [5–9] and R_K [10–12] anomalies by a similar amount in BSM effect [13,14].

Given that the $B \to K^{(*)}\ell^+\ell^-$ data suggest BSM effects in the muon modes rather than the electron modes, an interesting BSM candidate is a new gauge boson Z' of the gauged $L_\mu - L_\tau$ symmetry [15,16], the difference between the muon and tau numbers. The Z' boson couples to the muon but not to the electron. In Ref. [17], an extension of the gauged $L_\mu - L_\tau$ symmetry was constructed for the sake of introducing flavor-changing neutral current (FCNC) Z' couplings to the quark sector. In the model, the SM quarks mix with new vector-like quarks that are charged under the new gauge symmetry, leading to effective FCNC couplings of Z' with SM quarks. Among these, the left-handed (LH) bsZ' coupling gives rise to C_9^μ. The model provides a viable explanation for both the P_5' and R_K anomalies.

The gauged $L_\mu - L_\tau$ model is, however, just one possibility among many options for a UV theory. Hence, the model should be cross-checked using other methods, in particular, by direct searches at colliders. LHC phenomenology within the minimal version of the gauged $L_\mu - L_\tau$ model has been studied in Refs. [17–21], where Z' was searched for in $Z \to \mu^+\mu^- Z'(\to \mu^+\mu^-)$. The search is sensitive to Z' lighter than the Z boson and can probe the new gauge coupling g' as well as the Z' mass $m_{Z'}$. On the other hand, the extended model [17] gives effective Z' couplings to SM quarks, and these couplings could offer new ways to produce the Z' boson at colliders. In particular, the model predicts the existence of not only a LH tcZ' coupling that is directly related to the LH bsZ' coupling by $\mathrm{SU}(2)_L$ gauge symmetry, but also a right-handed (RH) tcZ' coupling. The authors of Refs. [17,22] have studied $t \to cZ'$ decay induced by these tcZ' couplings. This decay can be searched for in the huge number of $t\bar{t}$ events at the LHC; however, it becomes kinematically forbidden if the Z' mass

is greater than the mass difference between the top and charm quarks, i.e., for $m_{Z'} > m_t - m_c$.[1]

In this paper we consider another unique production mechanism of the Z' boson via the tcZ' couplings, namely, $cg \to tZ'$. To be specific, we study the following processes at the 14 TeV LHC: $pp \to tZ'$ (hereafter denoted as the tZ' process) and its conjugate $pp \to \bar{t}Z'$ (denoted as $\bar{t}Z'$) process, each followed by $Z' \to \mu^+\mu^-$ and $t \to bW^+(\to \ell^+\nu_\ell)$ (or its conjugate). A model-independent study of such tcZ'-induced processes at the LHC has been performed in Ref. [26].[2] We improve the treatment of SM background processes by including the ones missed in the previous study and find that the $\bar{t}Z'$ process is better suited for discovery than tZ' due to lower background. Combining the two signal processes (also referred to as the tZ' process collectively if there is no confusion), we present first the model-independent discovery potential of the tZ' process, aiming for the high-luminosity LHC (HL-LHC). In detailing our collider analysis, we choose two representative Z' mass values: just below (150 GeV) and above (200 GeV) the top-quark mass. We then extend the latter case to Z' masses up to 700 GeV, and reinterpret the model-independent results for RH tcZ' coupling within the gauged $L_\mu - L_\tau$ model [17]. It turns out that the LH tcZ' coupling implied by the $B \to K^{(*)}$ anomalies is rather small, and lies slightly beyond the discovery reach of the LHC even with 3000 fb^{-1} data. Therefore, we mainly focus on the RH tcZ' coupling, which is hardly probed by B physics. Yet our results can be easily translated into the case of the LH tcZ' coupling.

The model implies a flavor-conserving effective ccZ' coupling along with tcZ', while the effective Z' couplings containing the up quark, i.e., uuZ', cuZ', and tuZ', are suppressed by D meson constraints. The ccZ' coupling offers another production channel for Z' at the LHC, i.e., $c\bar{c} \to Z' \to \mu^+\mu^-$ (hereafter denoted as the dimuon process). Analogous to the tZ' case, we first perform a model-independent study, which is then reinterpreted within the gauged $L_\mu - L_\tau$ model. We find that the Z' can be discovered in either or both of the tZ' and dimuon processes. We show that the dimuon process has a better chance for discovery in most of the model parameter space, while simultaneously measuring the tZ' process can confirm the flavor structure of the Z' model.

The paper is organized as follows. In Sec. II, we briefly introduce the gauged $L_\mu - L_\tau$ model of Ref. [17] and give the effective Lagrangian for tcZ' and ccZ' couplings. We detail our collider analysis in Sec. III, which is divided into two subsections: the $\bar{t}Z'$ and tZ' processes induced by tcZ' coupling in Sec. III A, and the dimuon process induced by ccZ' coupling in Sec. III B. In Sec. III A, we also utilize existing LHC data [29] to illustrate its implication for tcZ' coupling. Three subsections are assigned to Sec. IV. In Sec. IV A we present the model-independent discovery reaches for RH tcZ' and ccZ' couplings at the HL-LHC. In Sec. IV B, we reinterpret the model-independent results within the gauged $L_\mu - L_\tau$ model. In Sec. IV C we discuss collider sensitivities to the LH tcZ' coupling, which is directly linked to the $B \to K^{(*)}$ anomalies. We summarize and offer further discussions in Sec. V.

II. MODEL

Let us briefly introduce the gauged $L_\mu - L_\tau$ model of Ref. [17], where a new U(1)′ gauge group associated with $L_\mu - L_\tau$ symmetry is introduced. The gauge and Higgs sectors of the U(1)′ consist of the gauge field Z' and the SM gauge singlet scalar field Φ, which carries unit charge under the U(1)′. The Φ field acquires a nonzero vacuum expectation value (VEV) $\langle\Phi\rangle = v_\Phi/\sqrt{2}$, which spontaneously breaks the U(1)′ and gives mass to Z', $m_{Z'} = g' v_\Phi$. In the minimal model, the Z' couples to the SM fermions through

$$\mathcal{L} \supset -g'(\bar{\mu}\gamma_\alpha\mu + \bar{\nu}_{\mu L}\gamma_\alpha\nu_{\mu L} - \bar{\tau}\gamma_\alpha\tau - \bar{\nu}_{\tau L}\gamma_\alpha\nu_{\tau L})Z'^\alpha. \quad (1)$$

In Ref. [17], an extended model was constructed by the addition of vector-like quarks $Q_L = (U_L, D_L)$, U_R, D_R and their chiral partners $\tilde{Q}_R = (\tilde{U}_R, \tilde{D}_R)$, $\tilde{U}_L$, $\tilde{D}_L$. The vector-like quarks carry +1 U(1)′ charge for $Q \equiv Q_L + \tilde{Q}_R$, and −1 for $U \equiv U_R + \tilde{U}_L$ and $D \equiv D_R + \tilde{D}_L$, with gauge-invariant mass terms given by

$$-\mathcal{L}_{\rm mass} = m_Q\bar{Q}Q + m_U\bar{U}U + m_D\bar{D}D. \quad (2)$$

The vector-like quarks mix with SM quarks via Yukawa interactions given by

$$-\mathcal{L}_{\rm mix} = \Phi\sum_{i=1}^{3}(\bar{\tilde{U}}_R Y_{Qu_i}u_{iL} + \bar{\tilde{D}}_R Y_{Qd_i}d_{iL}) + \Phi^\dagger\sum_{i=1}^{3}(\bar{\tilde{U}}_L Y_{Uui}u_{iR} + \bar{\tilde{D}}_L Y_{Ddi}d_{iR}) + \text{H.c.} \quad (3)$$

The $SU(2)_L$ symmetry relates the Yukawa couplings of LH up-type quarks to those of the LH down-type quarks:

$$Y_{Qu_i} = \sum_{i=1}^{3} V^*_{u_i d_j} Y_{Qd_j}, \quad (4)$$

where $i = 1, 2, 3$ and $V_{u_i d_j}$ is an element of the Cabibbo-Kobayashi-Maskawa (CKM) matrix.

At energy scales well below the heavy vector-like quark masses, the above Yukawa couplings generate an effective Lagrangian for FCNC Z' couplings to SM quarks,

[1]For $m_{Z'} > m_t + m_c$, $Z' \to tc$ [23–25] may happen, but its branching ratio is highly suppressed due to mixings between the heavy vector-like and SM quarks, in addition to rather low Z' production cross sections in the model we consider.

[2]A tuZ'-induced process $ug \to tZ'$ has also been studied with Z' decays to quarks in Refs. [27] ($Z' \to tj$) and [28] ($Z' \to b\bar{b}$).

$$\Delta\mathcal{L}_{\rm eff} = -Z'_\alpha \sum_{i,j=1}^{3} (g^L_{u_iu_j}\bar{u}_{iL}\gamma^\alpha u_{jL} + g^R_{u_iu_j}\bar{u}_{iR}\gamma^\alpha u_{jR} + g^L_{d_id_j}\bar{d}_{iL}\gamma^\alpha d_{jL} + g^R_{d_id_j}\bar{d}_{iR}\gamma^\alpha d_{jR}), \quad (5)$$

with

$$g^L_{u_iu_j} = g' \frac{Y^*_{Qu_i}Y_{Qu_j}v_\Phi^2}{2m_Q^2}, \qquad g^R_{u_iu_j} = -g' \frac{Y^*_{Uu_i}Y_{Uu_j}v_\Phi^2}{2m_U^2},$$
$$g^L_{d_id_j} = g' \frac{Y^*_{Qd_i}Y_{Qd_j}v_\Phi^2}{2m_Q^2}, \qquad g^R_{d_id_j} = -g' \frac{Y^*_{Dd_i}Y_{Dd_j}v_\Phi^2}{2m_D^2}. \quad (6)$$

Among these, the bsZ' couplings g^L_{sb} and g^R_{sb} affect the $b \to s\mu^+\mu^-$ transitions. In particular, g^L_{sb} gives a new contribution to the Wilson coefficient of the operator $(\bar{s}_L\gamma^\alpha b_L)(\bar{\mu}\gamma_\alpha\mu)$, given by

$$\Delta C^\mu_9 = \frac{g^L_{sb}g'}{m^2_{Z'}}, \quad (7)$$

which can explain both P'_5 and R_K anomalies. If the LH bsZ' coupling g^L_{sb} exists, the $\mathrm{SU}(2)_L$ relation in Eq. (4) would imply the existence of the LH tcZ' coupling g^L_{ct}. Unfortunately, the strength of g^L_{ct} favored by the P'_5 and R_K anomalies turns out to be below the discovery reach at HL-LHC, as we discuss in Sec. IV C.

The model, however, predicts the existence of the RH tcZ' coupling g^R_{ct}. The coupling is not directly linked to $B \to K^{(*)}$ transitions and is therefore hardly probed by B and K physics. But this coupling and its effect on top physics should be viewed on the same footing as the P'_5 and R_K anomalies. Because there is no gauge anomaly, it could even happen that the Q and D quarks are absent, or equivalently rather heavy, but the U quark could cause effects in the top/charm sector that are analogous to the current P'_5 and R_K "anomalies" in B decay, even if the latter "anomalies" disappear with more data. We therefore focus on the LHC phenomenology of the RH tcZ' coupling.

The RH tcZ' coupling is generated by the diagram shown in the left panel of Fig. 1 and is given by

$$g^R_{ct} = (g^R_{tc})^* = -g' \frac{Y^*_{Uc}Y_{Ut}v_\Phi^2}{2m_U^2}, \quad (8)$$

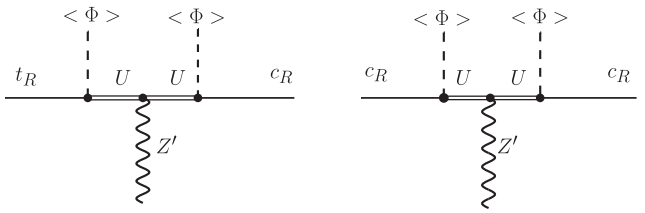

FIG. 1. Feynman diagrams that generate the effective RH tcZ' (left) and ccZ' (right) couplings.

which is nonzero only if $Y_{Uc} \neq 0$. One sees then that the diagram in the right panel of Fig. 1 generates the RH ccZ' coupling with

$$g^R_{cc} = -g' \frac{|Y_{Uc}|^2 v_\Phi^2}{2m_U^2}. \quad (9)$$

This means that if the RH tcZ' coupling exists, the RH ccZ' coupling should also exist. We shall therefore also consider the RH ccZ' coupling for LHC phenomenology.

In short, we consider the following effective Z' couplings in the collider study:

$$\Delta\mathcal{L}_{\rm eff} \supset -g^R_{cc}\bar{c}_R\gamma^\alpha c_R Z'_\alpha - (g^R_{ct}\bar{c}_R\gamma^\alpha t_R Z'_\alpha + \text{H.c.}), \quad (10)$$

with the model-dependent expressions of g^R_{ct} and g^R_{cc} in Eq. (8) and (9). But, our collider results can be straightforwardly applied to the LH counterparts, g^L_{ct} and g^L_{cc}.

In principle, the model could also give the effective couplings containing the up quark, i.e., the RH uuZ', cuZ', and tuZ' couplings, if Y_{Uu} is nonzero. In this case, $g^R_{uc} \propto |Y^*_{Uu}Y_{Uc}|$ is constrained by D-meson mixing and decays. We assume $Y_{Uu} = 0$ for simplicity, while RH ttZ' coupling is discussed in Sec. V. The presence of the U quark with nonzero Y_{Ut} and Y_{Uc} also leads to couplings of neutral SM bosons to the $t \to c$ currents. tcZ and tch couplings are induced at tree level, while $tc\gamma$ and tcg couplings (which are forbidden at tree level due to gauge symmetry) are generated at the one-loop level. In Ref. [17], it was claimed that the branching ratios of rare top-quark decays induced by these FCNC couplings with the SM bosons are suppressed over $\mathcal{B}(t \to cZ')$ by roughly a loop factor, with the latter assumed to be kinematically allowed.

We shall consider the mass range of 150 GeV $\leq m_{Z'} \leq$ 700 GeV, where the branching ratios and total width for Z' decay are nicely approximated by

$$\mathcal{B}(Z' \to \mu^+\mu^-) \simeq \mathcal{B}(Z' \to \tau^+\tau^-) \simeq \mathcal{B}(Z' \to \nu\bar{\nu}) \simeq \frac{1}{3},$$
$$\Gamma_{Z'} \simeq \frac{m^3_{Z'}}{4\pi v_\Phi^2} \simeq 0.75\ \text{GeV}\left(\frac{m_{Z'}}{150\ \text{GeV}}\right)^3\left(\frac{600\ \text{GeV}}{v_\Phi}\right)^2. \quad (11)$$

In this mass range, dominant constraints on the $(m_{Z'}, g')$ plane come from neutrino trident production and B_s mixing [17]. These can be recast into constraints on the VEV of the Φ field $v_\Phi (= m_{Z'}/g')$, which can be summarized as [22]

$$0.54\ \text{TeV} \lesssim v_\Phi \lesssim 5.6\ \text{TeV}\left(\frac{(34\ \text{TeV})^{-2}}{|\Delta C^\mu_9|}\right), \quad (12)$$

regardless of the value of $m_{Z'}$. The lower limit comes from neutrino trident production [19] with a 2σ range of the CCFR result [30],[3] while the upper limit is set by B_s mixing [32] with BSM effects allowed within 15% and the assumption that $m_Q \lesssim 10$ TeV. The upper limit becomes tighter for larger m_Q, e.g., $v_\Phi \lesssim 5.4(3.9)$ TeV $\times$ $[(34\ \text{TeV})^{-2}/|\Delta C_9^\mu|]$ for $m_Q = 20(50)$ TeV.

It is convenient to introduce the mixing parameters [22] between the vector-like quark U and RH top or charm quark defined by

$$\delta_{Uq} \equiv \frac{Y_{Uq} v_\Phi}{\sqrt{2} m_U}, \quad (q = t, c). \tag{13}$$

Small mixing parameters are assumed in obtaining the effective couplings of Eq. (8) and (9). In the following analysis, we allow the mixing strengths up to the Cabibbo angle, i.e., $|\delta_{Ut}|$, $|\delta_{Uc}| \le \lambda \simeq 0.23$, and the RH tcZ' coupling is constrained as

$$|g_{ct}^R| = \frac{m_{Z'}}{v_\Phi} |\delta_{Uc}||\delta_{Ut}| \lesssim 0.013 \times \left(\frac{m_{Z'}}{150\ \text{GeV}}\right)\left(\frac{600\ \text{GeV}}{v_\Phi}\right). \tag{14}$$

If the Yukawa couplings are hierarchical, e.g., $|Y_{Ut}| \gg |Y_{Uc}|$, this is further suppressed by $|Y_{Uc}/Y_{Ut}|$. A similar constraint holds for g_{cc}^R. These set the target ranges for the LHC study.

III. SEARCH FOR Z' AT THE LHC

A. tZ' and $\bar{t}Z'$ processes

The RH tcZ' coupling in Eq. (10) generates the parton-level process $cg \to tZ'$ through the Feynman diagrams in Fig. 2, leading to $pp \to tZ'$ at the LHC. We assume subsequent decays of $Z' \to \mu^+\mu^-$ and $t \to bW^+(\to \nu_\ell \ell^+)$ with $\ell = e$ or μ. In this subsection, we study the FCNC-induced process $pp \to tZ' \to b\nu_\ell \ell^+\mu^+\mu^-$ (tZ' process) and its conjugate process $pp \to \bar{t}Z' \to \bar{b}\bar{\nu}_\ell \ell^-\mu^+\mu^-$ ($\bar{t}Z'$ process) at the 14 TeV LHC, and analyze the prospect of discovering such a Z' boson. The RH tcZ' coupling also generates processes with an extra charm quark in the final states, i.e., $gg \to t\bar{c}Z'$ or $\bar{t}cZ'$. We will veto extra jets in the following analysis, but the latter processes can contribute to the signal region if the charm jet escapes detection. Hence, we also include the contributions from $gg \to t\bar{c}Z'/\bar{t}cZ'$ as a signal.

[3]The presence of the Z' boson affects couplings of the Z boson to the muon, tau, and corresponding neutrinos via the loop effect, which are constrained by experimental data taken at the Z resonance. A study in Ref. [17] showed that combining results from LEP and SLC [31] can provide competitive or slightly better limits than that from CCFR for $m_{Z'} \gtrsim 600$ GeV.

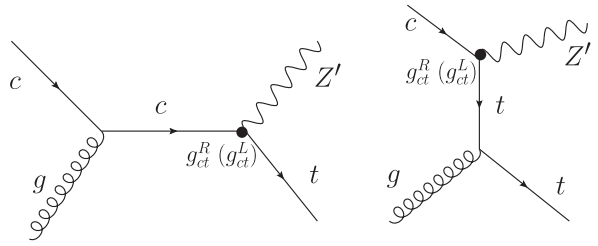

FIG. 2. Feynman diagrams contributing to $pp \to tZ'$.

For the sake of our collider analysis, we take two benchmark points for the effective theory defined by Eq. (10):

(1) Case A: $|g_{ct}^R| = 0.01$, $m_{Z'} = 150$ GeV.
(2) Case B: $|g_{ct}^R| = 0.01$, $m_{Z'} = 200$ GeV.

In Case A, where $m_{Z'} < m_t$, the $t \to cZ'$ decay is kinematically allowed with $\mathcal{B}(t \to cZ') \simeq 2 \times 10^{-5}$, and it contributes to $gg \to t\bar{c}Z'/\bar{t}cZ'$ via $gg \to t\bar{t}$. On the other hand, in Case B with $m_{Z'} > m_t$, the $t \to cZ'$ decay is kinematically forbidden.[4] Moreover, the behavior of event distributions for SM backgrounds is qualitatively different depending on whether the Z' mass is below or above the top-quark mass. The coupling value is in the range of Eq. (14) implied by the gauged $L_\mu - L_\tau$ model.

The signal cross sections are proportional to $|g_{ct}^R|^2 \times \mathcal{B}(Z' \to \mu^+\mu^-)$ if the Z' width is narrow. We assume $\mathcal{B}(Z' \to \mu^+\mu^-) = 1/3$, motivated by the gauged $L_\mu - L_\tau$ model, and $\Gamma_{Z'} \lesssim 1$ GeV for each case. Besides these assumptions, the analysis in this subsection is model independent. The effects of different Z' branching ratios can be taken into account by rescaling $|g_{ct}^R|$.

A similar BSM process $pp \to tZ \to \ell\nu b\ell^+\ell^-$ induced by tcZ couplings has been studied by the CMS experiment with 8 TeV data [29]. Our study closely follows this analysis. There exist several non-negligible SM backgrounds for the signal $b\nu_\ell \ell^+\mu^+\mu^-$ (tZ' process) and $\bar{b}\bar{\nu}_\ell \ell^-\mu^+\mu^-$ ($\bar{t}Z'$ process).

(1) *tZj and $\bar{t}Zj$ backgrounds*: The tZj background predominantly originates from

$$u + b \to t + Z + d \quad \text{or} \quad \bar{d} + b \to t + Z + \bar{u}, \tag{15}$$

with smaller contributions from c- or $\bar{s}$-initiated processes, while $\bar{t}Zj$ is generated by the charge-conjugate processes

[4]For $m_{Z'} > m_t$, a three-body decay $t \to c\mu^+\mu^-$ may still happen through an off-shell Z', and can contribute to the signal region via the $t\bar{t}$ events. In this case, the Z' mass cannot be reconstructed from the dimuon invariant mass, but the top-quark mass reconstruction may help discriminate signal and backgrounds. In Case B with $m_{Z'} = 200$ GeV, such a contribution is very tiny and is not included in our analysis, although it could be important for a Z' mass close to the top-quark mass.

$$d + \bar{b} \to \bar{t} + Z + u \quad \text{or} \quad \bar{u} + \bar{b} \to \bar{t} + Z + \bar{d}. \tag{16}$$

The tZj cross section is larger than $\bar{t}Zj$, as the parton distribution function (PDF) of the u quark is larger than the d quark in pp collisions [33]. Thus, the tZ' process suffers from larger background.

(2) $t\bar{t}Z$ *background*: $t\bar{t}Z$ becomes background for the $\bar{t}Z'$ (tZ') process, if the t ($\bar{t}$) decays hadronically and the $\bar{t}$ (t) decays leptonically, i.e., $t\bar{t}Z \to (bq\bar{q}')(\bar{b}\bar{\nu}_\ell\ell^-)(\mu^+\mu^-)$ $[(\bar{b}q'\bar{q})(b\nu_\ell\ell^+)(\mu^+\mu^-)]$, with some of the jets undetected. Indeed, $t\bar{t}Z$ constitutes a major part of the overall background.

(3) $t\bar{t}W$ *background*: $t\bar{t}W$ is another leading source of background. If the t, $\bar{t}$, and W all decay leptonically and a jet goes undetected, it can give the event topology with a trilepton ($\mu^+\mu^-\ell$), missing transverse energy ($\not{E}_T$) and a b-tagged jet. The $t\bar{t}W^+$ production cross section is larger than $t\bar{t}W^-$ [34] for pp collisions. Thus, the tZ' process again suffers larger background.

(4) WZ+*heavy-flavor jets and* WZ+ *light jets*: The WZ or $W\gamma^*$ production in association with heavy-flavor (h.f.) or light jets also contribute to background, if both W and Z/γ^* decay leptonically and a jet gets misidentified as a b-tagged jet. Here, the h.f. jet refers to the c jet. The rejection factors for the c jet and the light jet are taken to be 5 and 130, respectively [35]. The cross section for $W^+Z +$ light jets is larger than $W^-Z +$ light jets, while the $W^\pm Z$ production cross sections in association with h.f. jets are identical. This also gives larger background to the tZ' process than $\bar{t}Z'$.

We do not consider processes such as $t\bar{t}$, Drell-Yan (DY), or $W +$ jets, which could contribute to background if one or two nonprompt leptons are produced and reconstructed. These backgrounds are not properly modeled in simulations and require data for better estimation. The analysis of the similar process $pp \to tZ$ by CMS [29] showed that such processes provide subdominant contributions to the total background. In the case of the tZ' process, stricter cuts on the transverse momenta of the muons may reduce such contributions. These are beyond the scope of this paper.

The signal and background samples are generated at leading order (LO) in the pp collision with center-of-mass energy $\sqrt{s} = 14$ TeV, by the Monte Carlo event generator MadGraph5_aMC@NLO [36], interfaced to PYTHIA 6.4 [37] for showering. To include inclusive contributions, we generate the matrix elements of signal and backgrounds with up to one additional jet in the final state, followed by matrix element and parton shower merging with the MLM matching scheme [38]. Due to computational limitations, we do not include processes with two or more additional jets in the final state. The event samples are finally fed into the fast detector simulator Delphes 3.3.3 [39] for inclusion of (ATLAS-based) detector effects. The effective theory defined by Eqs. (1) and (10) is implemented by FeynRules 2.0 [40]. We adopt the PDF set CTEQ6L1 [41]. The LO $\bar{t}Zj$ and $t\bar{t}Z$ cross sections are normalized to the next-to-leading-order (NLO) ones by K-factors of 1.7 and 1.56, respectively [33]. For simplicity, we assume tZj has the same NLO K-factor as $\bar{t}Zj$. The NLO K-factor for the $t\bar{t}W^-$ ($t\bar{t}W^+$) process is taken to be 1.35 (1.27) [34]. The LO cross section for the $W^-Z +$ light jets background is normalized to the next-to-next-to-leading-order (NNLO) one by a factor of 2.07 [42]. We assume the same correction factor for $W^+Z +$ light jets and $W^\pm Z +$ h.f. jets for simplicity.

The signal cross sections for the tZ' and $\bar{t}Z'$ processes are identical, while some of the dominant (and the total) background cross sections are smaller for the latter process. The $\bar{t}Z'$ process is, therefore, better suited for discovering the Z'. It turns out that combining the tZ' and $\bar{t}Z'$ processes can improve discovery potential. In the following, we primarily investigate the $\bar{t}Z'$ process in showing details of our analysis, and finally give combined results of the tZ' and $\bar{t}Z'$ processes.

In Fig. 3 we present the normalized event distributions of the dimuon invariant mass $m_{\mu\mu}$ for the $\bar{t}Z'$ process in Cases A and B, and for the corresponding background contributions. The distributions are obtained by applying default cuts in MadGraph with minor modifications. In Figs. 4 and 5, the normalized p_T distributions are similarly shown for the leading and subleading muons, the third lepton, and the b-tagged jet, respectively.

We use two sets of cuts on the signal and background processes as explained below.

Preselection cuts: This set of cuts is used at the generator level. The leading, subleading, and third leptons in an event are required to have a minimum p_T of 60, 30, and 15 GeV, respectively, in both Cases A and B. The

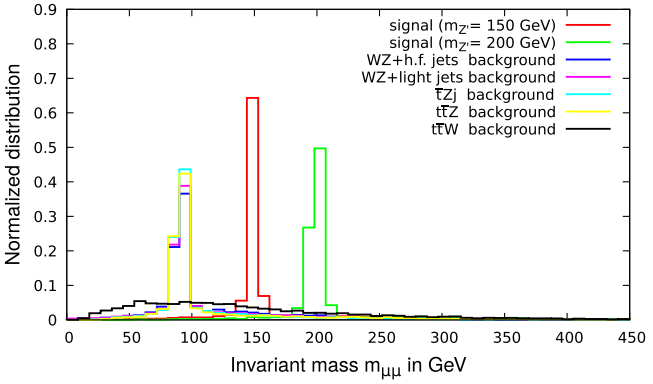

FIG. 3. Normalized distributions of the dimuon invariant mass for the $\bar{t}Z'$ process in Cases A ($m_{Z'} = 150$ GeV) and B ($m_{Z'} = 200$ GeV), and for the corresponding backgrounds, with close-to-default cuts in MadGraph.

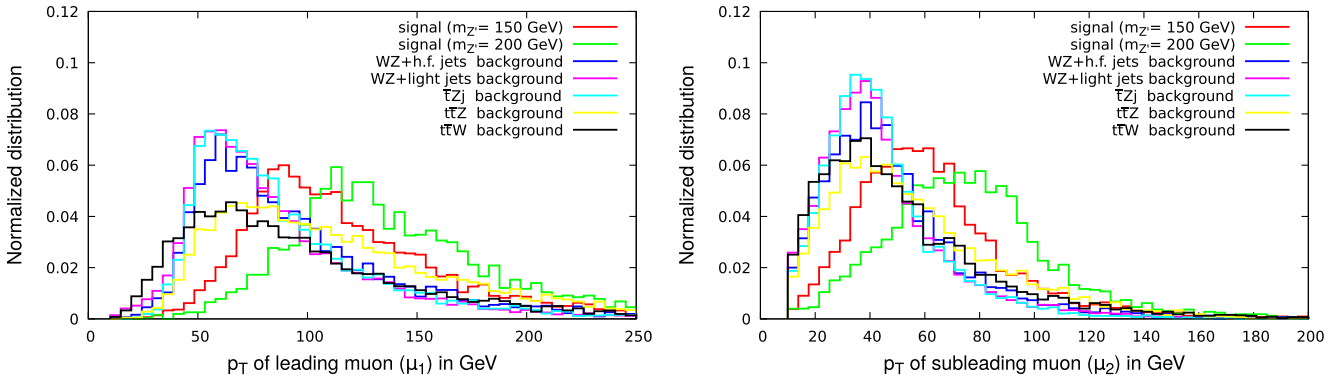

FIG. 4. Normalized p_T distributions for the leading (left) and subleading (right) muons, for the $\bar{t}Z'$ process and its backgrounds as in Fig. 3.

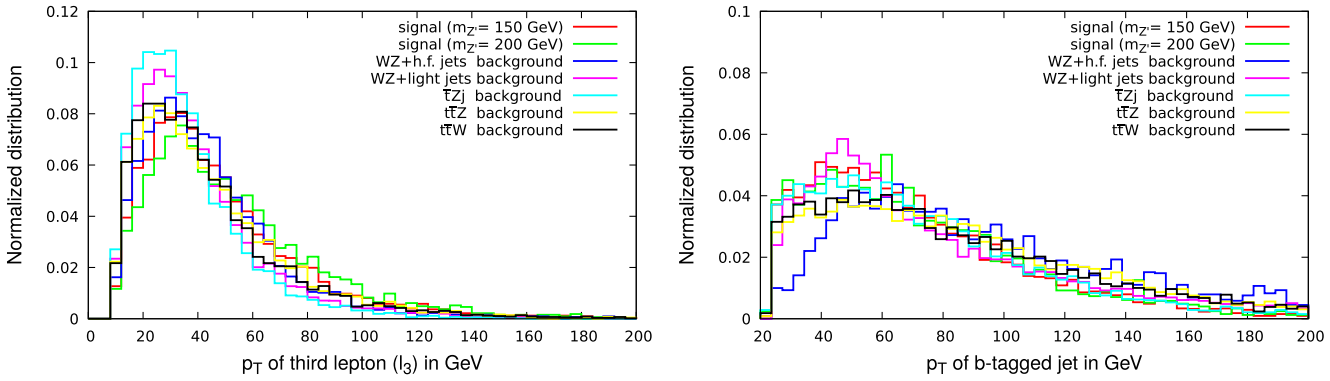

FIG. 5. Normalized p_T distributions for the third lepton (left) and b-tagged jet (right), for the $\bar{t}Z'$ process and its backgrounds as in Fig. 3.

maximum pseudorapidity of all leptons are required to be $|\eta^{\ell}| < 2.5$. The transverse momentum of jets are required to be greater than 20 GeV. The minimum separation between the two oppositely charged muons is required to be $\Delta R > 0.4$. The rest of the cuts are set to their default values in MadGraph.

Selection cuts: Utilizing the signal and background distributions in Figs. 3, 4, and 5, we impose a further set of cuts. Events are selected such that each should contain three (at least two muon-type) leptons and at least one b-tagged jet. Jets are reconstructed by the anti-k_T algorithm with radius parameter $R = 0.5$. Stricter cuts on lepton transverse momenta are applied: the leading muon, subleading muon, and third lepton in an event are required to have a minimum p_T of 60 (75), 30 (45), and 20 (20) GeV, respectively, in Case A (B). The third lepton is assumed to arise from the top-quark decay accompanied by missing transverse energy $\not{E}_T$ and a b jet. We require that $\not{E}_T > 30$ GeV and the reconstructed W boson mass $m_T^W > 10$ GeV. The leading b-tagged jet is required to have $p_T > 20$ GeV. An event is rejected if the p_T of the subleading jet or subleading b-tagged jet is greater than 20 GeV. This veto significantly reduces the $t\bar{t}Z$ and $t\bar{t}W$ backgrounds, as both processes contain two b jets from the decay of the t and $\bar{t}$. We will also analyze the impact of removing such a jet veto shortly. We finally apply the invariant mass cut $|m_{\mu\mu} - m_{Z'}| < 15$ GeV on two oppositely charged muons. If an event contains three muons, there are two ways to make a pair of two oppositely charged muons. In such a case, we identify the pair having the invariant mass $m_{\mu\mu}$ closer to $m_{Z'}$ as the one coming from the Z' decay, and impose the above invariant mass cut on this pair.

The effects of these two sets of cuts on the signal and background processes are illustrated in Table I for Case A, and Table II for Case B. From these tables, we see that the selection cuts significantly reduce the number of background events (B), and the number of signal events (S) becomes larger than B for the $\bar{t}Z'$ process in both Cases A and B. The expected numbers of events with integrated luminosity $\mathcal{L} = 300$ fb^{-1} are $S \simeq 26(11)$ and $B \simeq 17(9)$ in Case A (B) for the $\bar{t}Z'$ process. For comparison, the effects of removing the veto on the subleading jet are also shown in the tables. Without the jet veto, the signal events slightly increase as $S \simeq 27(12)$, but the background events increase more as $B \simeq 27(14)$ in Case A (B) for the $\bar{t}Z'$ process. This

TABLE I. Effects of two sets of cuts on cross sections (in fb) for the $\bar{t}Z'$ and SM background processes in Case A ($m_{Z'} = 150$ GeV). The effect of the selection cuts without the subleading jet veto is also shown. (See text for details.) The second column gives the signal process, while the effects on individual backgrounds are tabulated in the third to seventh columns. Cross sections for backgrounds of the conjugate process tZ' are given in parentheses, if they differ from the case of the $\bar{t}Z'$ process: tZj (third column), $t\bar{t}W^+$ (fifth column), and $W^+Z +$ light jets (sixth column), where similar sets of cuts as the $\bar{t}Z'$ process are applied. The last column shows the sum of all background cross sections.

Cuts	Signal (Case A)	$\bar{t}Zj$	$t\bar{t}Z$	$t\bar{t}W^-$	$W^-Z +$ light jets	$W^-Z +$ h.f. jets	Total BG
Preselection cuts	0.410	0.872 (1.552)	1.672	0.514 (1.384)	0.641 (0.868)	4.55	8.25 (10.03)
Selection cuts (No jet veto)	0.090	0.012 (0.022)	0.026	0.023 (0.071)	0.012 (0.015)	0.017	0.090 (0.151)
Selection cuts	0.085	0.011 (0.020)	0.014	0.014 (0.039)	0.005 (0.007)	0.014	0.058 (0.094)

TABLE II. Same as Table I, but for Case B ($m_{Z'} = 200$ GeV).

Cuts	Signal (Case B)	$\bar{t}Zj$	$t\bar{t}Z$	$t\bar{t}W^-$	$W^-Z +$ light jets	$W^-Z +$ h.f. jets	Total BG
Preselection cuts	0.186	0.872 (1.552)	1.672	0.514 (1.384)	0.641 (0.868)	4.55	8.25 (10.03)
Selection cuts (No jet veto)	0.040	0.006 (0.010)	0.014	0.012 (0.035)	0.005 (0.007)	0.008	0.045 (0.074)
Selection cuts	0.037	0.005 (0.009)	0.007	0.008 (0.021)	0.002 (0.003)	0.007	0.029 (0.047)

illustrates the advantage of imposing the veto on the subleading jet.

To estimate the signal significance, we use [43]

$$\mathcal{Z} = \sqrt{2[(S+B)\ln(1+S/B) - S]}. \tag{17}$$

This takes the well-known $\mathcal{Z} \simeq S/\sqrt{B}$ form for $S \ll B$, but it does not hold in the current case. We require $\mathcal{Z} \geq 5$ for 5σ discovery. In Case A (B), therefore, the Z' can be discovered at 5σ in the $\bar{t}Z'$ process with integrated luminosity $\mathcal{L} = 290(730)$ fb^{-1}. Discovery in the tZ' process would require more data: $\mathcal{L} = 410(1060)$ fb^{-1} in Case A (B). Combining the tZ' and $\bar{t}Z'$ processes, one could discover the Z' with lower integrated luminosities: $\mathcal{L} = 180(450)$ fb^{-1} in Case A (B). Therefore, better discovery potential is attained with the combined tZ' and $\bar{t}Z'$ processes. In the following, we will give results for this combined case and also refer to it as the tZ' process collectively if there is no confusion.

Before closing this subsection, we briefly discuss the use of some existing LHC data to search for the tcZ' coupling. The CMS Collaboration [29] has studied the SM process $pp \to tZq$ in the three-lepton (electron or muon) final state with 8 TeV data, measuring the cross section $\sigma(pp \to tZq \to \ell\nu b\ell^+\ell^- q) = 10^{+8}_{-7}$ fb, which is consistent with the SM prediction of 8.2 fb. Taking this as background, the CMS Collaboration has also searched for the BSM process $pp \to tZ$ induced by tqZ ($q = u, c$) couplings; no evidence was found, resulting in the 95% C.L. upper limits of $\mathcal{B}(t \to uZ) < 0.022\%$ and $\mathcal{B}(t \to cZ) < 0.049\%$.

In the CMS analysis [29], tZq production has been searched for with the invariant mass cut of $76\ \text{GeV} < m_{\ell\ell} < 106\ \text{GeV}$ on two oppositely charged same-flavor leptons. Hence, the search is sensitive to the tZ' process if the Z' mass falls into this window. The measured cross section for the three-muon channel is $\sigma(pp \to tZq \to \mu\nu b\mu^+\mu^- q) = 5^{+9}_{-5}$ fb, while the SM prediction is around 2.1 fb with an uncertainty of less than 10%. Following the same event selection cuts as the CMS analysis, we calculate the Z' contribution to be 17.4 fb $\times\, |g^R_{ct}/0.05|^2$ for $m_{Z'} = 95$ GeV by MadGraph followed by showering and incorporating CMS-based detector effects. Symmetrizing the experimental uncertainties by naive average and allowing the Z' effect to enhance the cross section up to 2σ of the measured value, we obtain an upper limit of $|g^R_{ct}| \lesssim 0.05$ for $m_{Z'} \sim m_Z$.

B. Dimuon process: $pp \to Z' + X \to \mu^+\mu^- + X$

The flavor-conserving ccZ' coupling g^R_{cc} in Eq. (10) gives rise to the parton-level process $c\bar{c} \to Z'$. Thus, the Z' can also be searched for via $pp \to Z' + X \to \mu^+\mu^- + X$ (dimuon process), where existing dimuon resonance search results at the LHC can already constrain $|g^R_{cc}|$. The experimental searches do not veto extra activities X; hence, we also include subdominant contributions from $cg \to cZ'$ and $gg \to c\bar{c}Z'$ processes, induced by the RH ccZ' coupling. In the following analysis, we adopt the 13 TeV results from the ATLAS [44] and CMS collaborations [45] (both based on ~13 fb^{-1} data). The ATLAS analysis puts 95% C.L. upper limits on the Z' production cross section times $Z' \to \mu^+\mu^-$ branching ratio for $150\ \text{GeV} \lesssim m_{Z'} \lesssim 5$ TeV, while the CMS analysis provides 95% C.L. upper limits on the quantity R_σ, which is defined as the ratio of the dimuon production cross section via Z' to the one via Z or

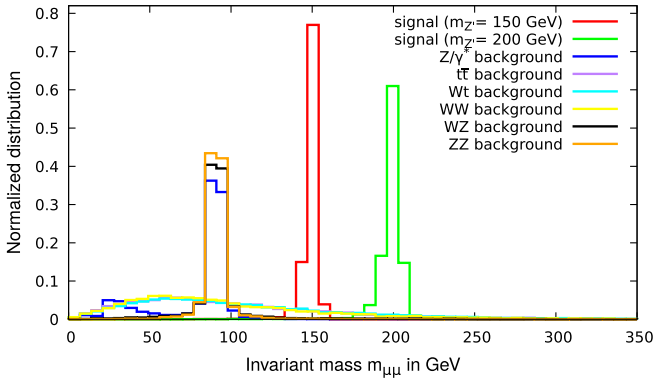

FIG. 6. Normalized distributions of the dimuon invariant mass for the dimuon process $pp \to Z' + X \to \mu^+\mu^- + X$ in Cases I ($m_{Z'} = 150$ GeV) and II ($m_{Z'} = 200$ GeV) and for the backgrounds, with close-to-default cuts in MadGraph.

γ^* (in the dimuon-invariant-mass window of 60–120 GeV), for 400 GeV $\lesssim m_{Z'} \lesssim 4.5$ TeV. We interpret the latter as the limits on

$$R_\sigma = \frac{\sigma(pp \to Z' + X)\mathcal{B}(Z' \to \mu^+\mu^-)}{\sigma(pp \to Z + X)\mathcal{B}(Z \to \mu^+\mu^-)}, \qquad (18)$$

and convert them into the limits on $\sigma(pp \to Z' + X)\mathcal{B}(Z' \to \mu^+\mu^-)$ by multiplying the SM prediction $\sigma(pp \to Z + X)\mathcal{B}(Z \to \mu^+\mu^-) = 1928.0$ pb [46]. With parameters allowed by these searches, we study the prospect of discovering the dimuon process at the 14 TeV LHC.

As in the previous subsection, we choose two benchmark points:

(1) Case I: $|g^R_{cc}| = 0.005$, $m_{Z'} = 150$ GeV.
(2) Case II: $|g^R_{cc}| = 0.005$, $m_{Z'} = 200$ GeV.

We assume a narrow Z' width ($\Gamma_{Z'} \lesssim 1$ GeV) and $\mathcal{B}(Z' \to \mu^+\mu^-) = 1/3$ for each case. The benchmark points are allowed by the dimuon resonance searches, as can be seen from the right panel of Fig. 8 in the next section.

For the treatment of SM backgrounds, we follow the analysis of the ATLAS Collaboration [44]. There are multiple sources of backgrounds. The dominant contribution arises from the DY process, where the muon pair is produced via Z/γ^*. Other non-negligible contributions arise from $t\bar{t}$, Wt, and WW production, while contributions from WZ and ZZ production are less significant. As in the tZ' case, we do not include backgrounds associated with nonprompt leptons.

The signal and background samples for the dimuon process are generated in a similar way as in the previous subsection, except for the treatment of additional jets. In this case, we generate matrix elements of signal and backgrounds with up to two additional jets, followed by showering. The LO Z/γ^* (DY) cross section is normalized to the NNLO QCD + NLO EW one with the LO photon-induced channel by the correction factor 1.27. The latter is obtained using FEWZ 3.1[47] in the dimuon-invariant-mass range of $m_{\mu\mu} > 106$ GeV. The LO $t\bar{t}$ and Wt cross sections are normalized to the NNLO + NNLL ones by the factors 1.84 [48] and 1.35 [49], respectively. As for WW, WZ, and ZZ, the LO cross sections are normalized to the NNLO QCD ones by the factors 1.98 [50], 2.07 [42], and 1.74 [51], respectively.

Normalized distributions of the dimuon invariant mass $m_{\mu\mu}$ are given in Fig. 6 for the dimuon process in Cases I and II and the backgrounds, obtained by close-to-default cuts in MadGraph. The p_T distributions of the leading and subleading muons are given in Fig. 7. We apply two sets of cuts on signal and background events as in the previous subsection.

Preselection cuts: The two muons in an event are required to have transverse momenta $p_T^\mu > 50$ GeV and maximum pseudorapidity $|\eta|^\mu < 2.5$, with a minimum separation $\Delta R > 0.4$.

Selection cuts: Events are selected such that each event contains two oppositely charged muons with leading muon transverse momentum $p_T^{\mu_1} > 60(75)$ GeV, and subleading muon $p_T^{\mu_2} > 55(60)$ GeV in Case I (II). We impose an

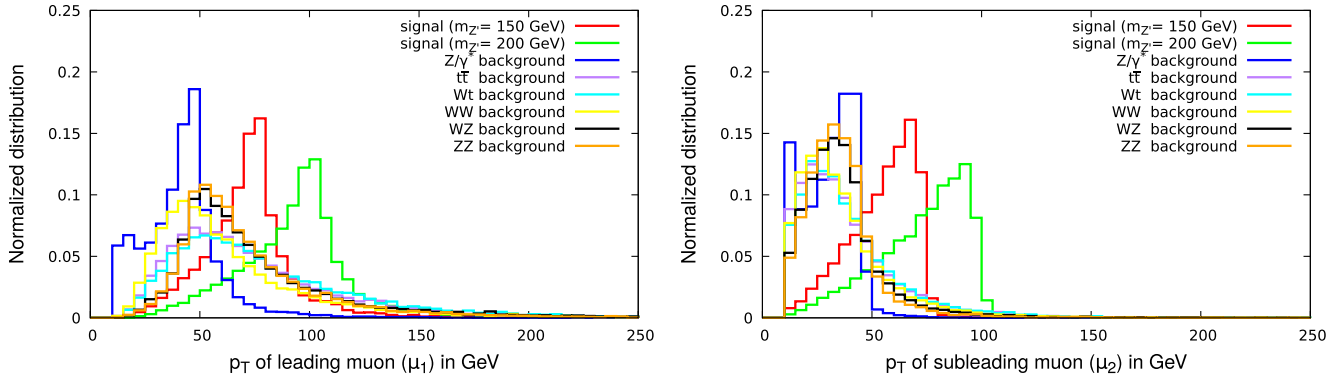

FIG. 7. Normalized p_T distributions for leading (left) and subleading (right) muons, for the dimuon process and its backgrounds as in Fig. 6.

TABLE III. Same as Table I (cross sections in fb), but for the dimuon process in Case I ($m_{Z'} = 150$ GeV).

Cuts	Signal (Case I)	Z/γ^*	$t\bar{t}$	Wt	WW	WZ	ZZ	Total BG
Preselection cuts	38.65	19980	1785	166	212	128.44	74.82	22346
Selection cuts	20.96	1677	163	16	24	0.22	0.02	1880

TABLE IV. Same as Table I, but for the dimuon process in Case II ($m_{Z'} = 200$ GeV).

Cuts	Signal (Case II)	Z/γ^*	$t\bar{t}$	Wt	WW	WZ	ZZ	Total BG
Preselection cuts	17.77	19980	1785	166	212	128.44	74.82	22346
Selection cuts	10.22	532	117	12	14	0.12	0.01	675

invariant-mass cut of $|m_{\mu\mu} - m_{Z'}| < 15$ GeV on the two muons in both Cases I and II.

The effects of the two sets of cuts on the signal and backgrounds are tabulated in Table III for Case I, and in Table IV for Case II. From these tables, we see that the number of background events B is significantly larger than the signal events S in both Cases I and II, even after the selection cuts. In this case, the signal significance of Eq. (17) becomes $\mathcal{Z} \simeq S/\sqrt{B}$, which we use to estimate the discovery potential of the dimuon process. We find that the Z' in benchmark Case I (II) can be discovered in the dimuon process at 5σ with an integrated luminosity of $\mathcal{L} = 110(170)$ fb^{-1}. We remark that in actual experimental searches the Z' mass would be scanned over a certain range and the look-elsewhere effect would be included. The latter effect will reduce the signal significance we estimated, pushing the integrated luminosities required for discovery to higher values.

IV. DISCOVERY POTENTIAL

In this section, we first extend the results of the previous section to higher Z' masses within the effective theory framework of the RH tcZ' and ccZ' couplings, then give the discovery potential of the Z' in the tZ' and dimuon processes at the 14 TeV LHC. We then reinterpret these model-independent results based on the gauged $L_\mu - L_\tau$ model [17]. We also discuss the sensitivity of the LH tcZ' coupling that is directly linked to the P_5' and R_K anomalies.

A. Model-independent results

In the previous section, we studied the tZ' and dimuon processes for $m_{Z'} = 150$ and 200 GeV with benchmark values of the effective couplings g_{ct}^R and g_{cc}^R. In this subsection, we extend the analysis to higher Z' masses up to 700 GeV and to arbitrary values of g_{ct}^R and g_{cc}^R, and illustrate the Z' discovery potential at the 14 TeV LHC with 300 and 3000 fb^{-1} integrated luminosities.

For $m_{Z'} = 150$ and 200 GeV, we simply rescale the results of the previous section by $|g_{ct}^R|$ and $|g_{cc}^R|$. For higher Z' masses from 300 to 700 GeV, in steps of 100 GeV, we follow the same method as in the 200 GeV case for the generation of events and the application of cuts. In particular, we adopt the same dimuon-invariant-mass cut of $|m_{\mu\mu} - m_{Z'}| < 15$ GeV. We choose a Z' width such that $\Gamma_{Z'}/m_{Z'} \lesssim 1\%$ is satisfied for each mass. We assume $\mathcal{B}(Z' \to \mu^+\mu^-) = 1/3$.

We do not consider lower Z' masses, as controlling SM backgrounds becomes more difficult when $m_{Z'} \sim m_Z$. We leave this case for future analysis. We restrict the analysis for the Z' mass up to 700 GeV, as the S and B for the tZ' process [obtained from Eq. (17) with 5σ] get smaller than $\mathcal{O}(1)$ beyond this mass. On the other hand, for the dimuon process, the S/B ratios become very low for masses beyond 700 GeV, and a proper understanding of systematic uncertainties would be needed.

The discovery reach for the effective couplings g_{ct}^R and g_{cc}^R are shown in the left and right panels of Fig. 8, respectively, for 150 GeV $\leq m_{Z'} \leq$ 700 GeV. In the left panel, the upper red (lower blue) solid line represents the 5σ discovery reach for the tZ' process with 300(3000) fb^{-1} integrated luminosity, while the corresponding dashed lines represent the 3σ reach. In the right panel, the discovery reaches for the dimuon process are similarly shown; in this case, existing LHC results for dimuon resonance searches already constrain g_{cc}^R, as discussed in Sec. III B, and the 95% C.L. exclusion set by ATLAS [44] (CMS [45]) with around 13 fb^{-1} of 13 TeV data is shown by the gray (semitransparent blue) shaded region.

We see that, at the 14 TeV LHC with 300(3000) fb^{-1} data, the tZ' process can be discovered for $|g_{ct}^R| = 0.025$ up to $m_{Z'} \simeq 490(700)$ GeV; the dimuon process can be discovered for $|g_{cc}^R| = 0.01$ up to $m_{Z'} \simeq 460(650)$ GeV. We also read the discovery reach for representative Z' mass values: $|g_{ct}^R| \gtrsim 0.0086(0.0047)$ and $|g_{cc}^R| \gtrsim 0.0039(0.0022)$ for $m_{Z'} = 150$ GeV; $|g_{ct}^R| \gtrsim 0.026(0.013)$ and $|g_{cc}^R| \gtrsim 0.011(0.0063)$ for $m_{Z'} = 500$ GeV, with 300(3000) fb^{-1} data. The dimuon process can probe smaller Z' couplings than the tZ' process, but these two couplings are independent in general.

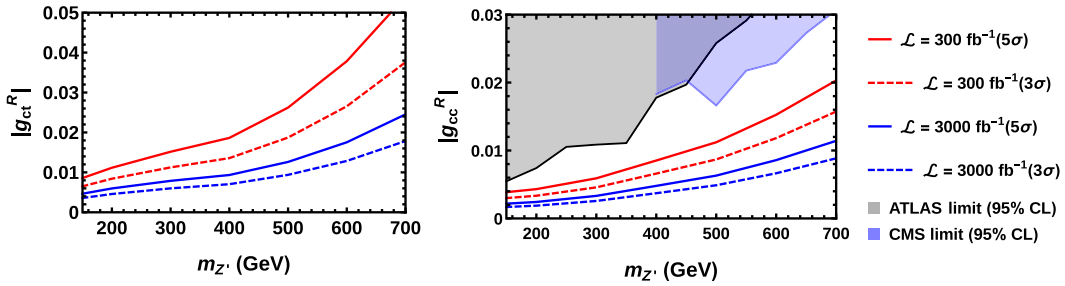

FIG. 8. Left: 5σ discovery reach in $|g_{ct}^R|$ strength vs $m_{Z'}$ for the combination of the $pp \to tZ'$ and $\bar{t}Z'$ processes at the 14 TeV LHC with 300 fb^{-1} (upper red solid line) or 3000 fb^{-1} (lower blue solid line) data, and the corresponding 3σ reach shown by dashed lines. Right: Same as the left panel, but for $|g_{cc}^R|$ vs $m_{Z'}$ for the dimuon process $pp \to Z' + X \to \mu^+\mu^- + X$. The gray (semitransparent blue) shaded region is excluded at 95% C.L. by the ATLAS's dimuon resonance search [44] (CMS [45]) with ~13 fb^{-1} data at the 13 TeV LHC. $\mathcal{B}(Z' \to \mu^+\mu^-) = 1/3$ and $\Gamma_{Z'}/m_{Z'} \lesssim 1\%$ are assumed in both panels.

The results in Fig. 8 are model independent, except for the assumptions of a narrow Z' width and $\mathcal{B}(Z' \to \mu^+\mu^-) = 1/3$, which are motivated by the gauged $L_\mu - L_\tau$ model. For arbitrary $\mathcal{B}(Z' \to \mu^+\mu^-)$, the discovery reach can be obtained from Fig. 8 by simply replacing

$$|g_{ct}^R| \to |g_{ct}^R|\sqrt{3 \times \mathcal{B}(Z' \to \mu^+\mu^-)}, \tag{19}$$

with a similar replacement for $|g_{cc}^R|$. We remark that the same results apply to the LH coupling g_{ct}^L (g_{cc}^L) if the RH coupling g_{ct}^R (g_{cc}^R) is set to zero.

B. Interpretation in the gauged $L_\mu - L_\tau$ model

Both the tZ' and dimuon processes can probe the effective Z' couplings implied by the gauged $L_\mu - L_\tau$ model [17]. In this subsection, we reinterpret the model-independent results of the previous subsection within the gauged $L_\mu - L_\tau$ model[5] through the expressions for g_{ct}^R and g_{cc}^R in Eqs. (8) and (9), and discuss the discovery potential at the 14 TeV LHC with 3000 fb^{-1} data.

From Eq. (14), one can observe that a smaller v_Φ is better probed for fixed $m_{Z'}$ and mixing parameters δ_{Ut} and δ_{Uc}. Applying the 5σ discovery reach of Fig. 8, we find that the tZ' process can be discovered for $m_{Z'} = 150(500)$ GeV with $\delta_{Ut} = \delta_{Uc} = \lambda \simeq 0.23$ if $v_\Phi \lesssim 1.7(2.0)$ TeV; the dimuon process can be discovered for the same parameters if $v_\Phi \lesssim 3.6(4.2)$ TeV. In general, if the two Yukawa couplings have the same value, i.e., $\delta_{Uc}/\delta_{Ut} = Y_{Uc}/Y_{Ut} = 1$, we find that the dimuon process has better discovery potential. If the Yukawa couplings are hierarchical such that $Y_{Uc}/Y_{Ut} = \lambda$, the discovery reach of the tZ' process becomes $v_\Phi \lesssim 390(470)$ GeV, which is better than the dimuon process $v_\Phi \lesssim 190(220)$ GeV for $m_{Z'} = 150(500)$ GeV with $\delta_{Ut} = \lambda$. These v_Φ values are, however, already excluded by the neutrino trident production [see Eq. (12)]. Taking a milder hierarchy such that $Y_{Uc}/Y_{Ut} \simeq 0.47(0.48)$, we find a comparable discovery reach between the two processes: $v_\Phi \lesssim 790(990)$ GeV for $m_{Z'} = 150(500)$ GeV with $\delta_{Ut} = \lambda$. In this case, the two processes can probe the parameter region allowed by the neutrino trident production. For a slightly smaller Y_{Uc}/Y_{Ut}, the tZ' process can have better discovery potential than the dimuon process while satisfying the neutrino trident production constraint.

The mixing parameters δ_{Ut} and δ_{Uc}, defined in Eq. (13), depend on Y_{Ut}, Y_{Uc}, m_U as well as $v_\Phi (= m_{Z'}/g')$. In Fig. 9, we show the impact of the Yukawa couplings on the discovery of the Z' by taking $v_\Phi = 600$ GeV, close to the lower end of Eq. (12), to maximize the discovery reach. We also fix $m_U = 3$ TeV, but different choices of m_U will just give rescaled figures.

In the left panel of Fig. 9, the discovery reach is given in the Y_{Ut}–Y_{Uc} plane for $m_{Z'} = 150$ GeV. The red and horizontal blue solid lines represent the discovery reach for the tZ' and dimuon processes, respectively. We only consider the parameter region where the mixing parameters satisfy $|\delta_{Ut}|, |\delta_{Uc}| \le \lambda$, shown by the vertical dotted and horizontal dashed lines, respectively. The gray shaded region represents the 95% C.L. exclusion from ATLAS's dimuon resonance search [44]. The latter can already probe the parameter region that satisfies $|\delta_{Uc}| \le \lambda$. The dimuon process can be discovered for $Y_{Uc} \gtrsim 0.7$, and generally has a larger discovery zone than the tZ' process, in particular for small Y_{Ut}. Interestingly, there is an overlap of discovery zones of the two processes for $Y_{Ut} \gtrsim 0.9$ and $Y_{Uc} \gtrsim 0.7$, and discovery might be possible for both processes. This might be useful to probe the flavor structure of the model. As the Z' is lighter than the top quark, $t \to cZ'$ may happen. The green dash-dotted contours are plotted for $\mathcal{B}(t \to cZ') = 10^{-6}$ and 10^{-5}. One can see that the tZ' process can probe the region where $\mathcal{B}(t \to cZ') < 10^{-5}$.

[5]In the gauged $L_\mu - L_\tau$ model, a nonzero g_{ct}^R is accompanied with a nonzero g_{tt}^R, leading to the $gg \to t\bar{t}Z'$ process. The latter could contribute to the signal region of the tZ' process despite the veto on extra jets. We, however, found that such a contribution is smaller than 1% for $|g_{ct}^R| \sim |g_{tt}^R|$. We ignore the effects from the $t\bar{t}Z'$ production in the following analysis.

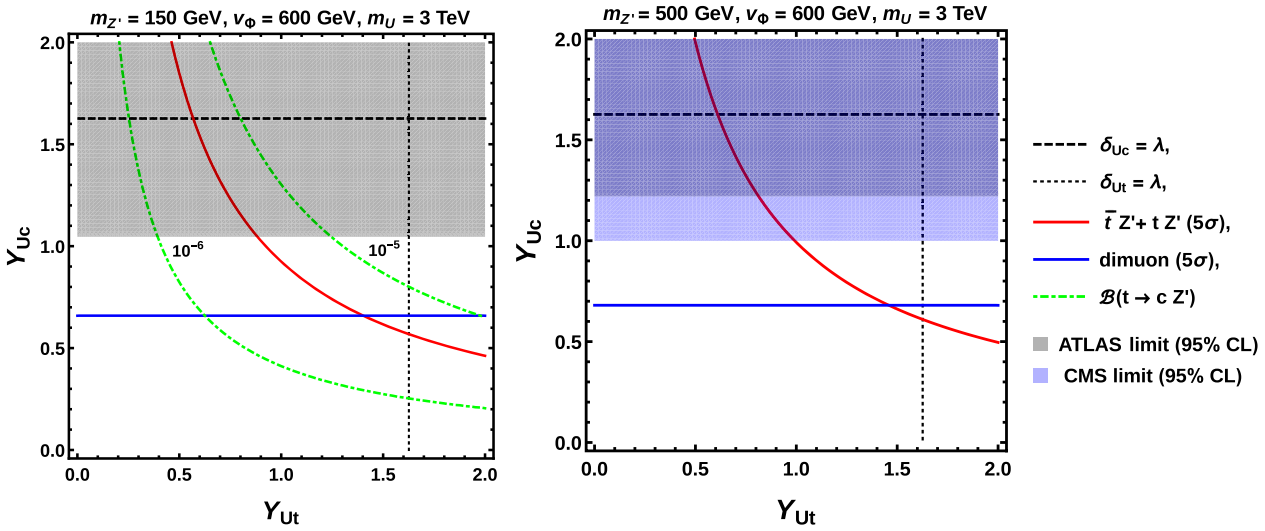

FIG. 9. Left: 5σ discovery reach in the Y_{Ut}–Y_{Uc} plane for $m_{Z'} = 150$ GeV with $v_\Phi = 600$ GeV ($\Gamma_{Z'} \simeq 0.74$ GeV) and $m_U = 3$ TeV with 3000 fb^{-1} data: the red solid line represents the tZ' process, and the horizontal blue solid line represents the dimuon process. Green dash-dotted lines are contours for $\mathcal{B}(t \to cZ') = 10^{-6}$ and 10^{-5}. The gray shaded region is the 95% C.L. exclusion by the ATLAS dimuon resonance search [44]. The mixing parameter δ_{Ut} (δ_{Uc}) exceeds $\lambda \simeq 0.23$ beyond the vertical dotted (horizontal dashed) line. Right: Same as the left panel, but for $m_{Z'} = 500$ GeV ($\Gamma_{Z'} \simeq 27$ GeV). The CMS [45] 95% C.L. exclusion, shown by the semitransparent blue shaded region, is overlaid on the gray shaded ATLAS exclusion and gives a stronger constraint.

In the right panel of Fig. 9, a similar plot is shown for $m_{Z'} = 500$ GeV. We again take $v_\Phi = 600$ GeV, which gives a Z' width of $\Gamma_{Z'} \simeq 27$ GeV. This is rather large and the dimuon-invariant-mass distribution would spread outside the invariant mass cut $|m_{\mu\mu} - m_{Z'}| < 15$ GeV, applied in our collider study of the last subsection with the narrow-width assumption. Hence, the discovery reaches shown in the last subsection do not apply. In order to evaluate the discovery potential in this case, we regenerated the signal events for the case of $m_{Z'} = 500$ GeV with $\Gamma_{Z'} \simeq 27$ GeV and redid the cut-based analysis with the same cuts as the narrow-width case, but relaxing the invariant mass cut to $|m_{\mu\mu} - m_{Z'}| < 55$ GeV. We then obtain the model-independent discovery reach

$$|g^R_{ct}| \gtrsim 0.016, \qquad |g^R_{cc}| \gtrsim 0.0077 \quad (\Gamma_{Z'} = 27\ \text{GeV}) \tag{20}$$

at $m_{Z'} = 500$ GeV for 3000 fb^{-1} data. The result gets slightly worse due to the increased number of SM

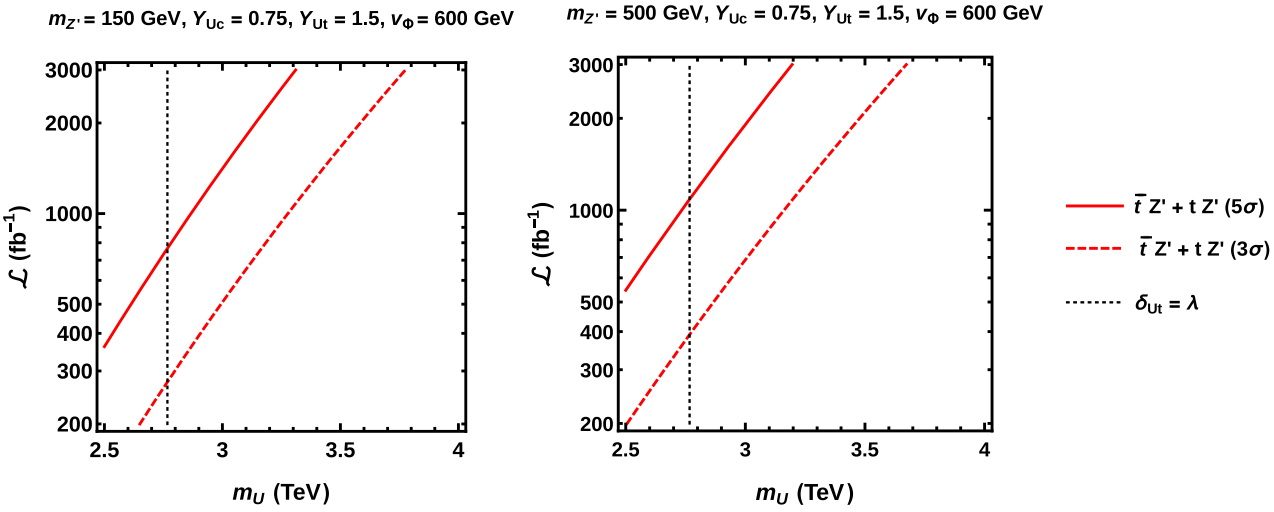

FIG. 10. Integrated luminosities needed for 5σ discovery (red solid lines) of the tZ' process at the 14 TeV LHC as a function of the vector-like quark mass m_U with $Y_{Ut} = 1.5$, $Y_{Uc} = 0.75$, and $v_\Phi = 600$ GeV, for $m_{Z'} = 150$ GeV (left) and 500 GeV (right). The 3σ reach is given by red dashed lines, while vertical dotted lines indicate the m_U value below which the mixing parameter δ_{Ut} exceeds $\lambda \simeq 0.23$.

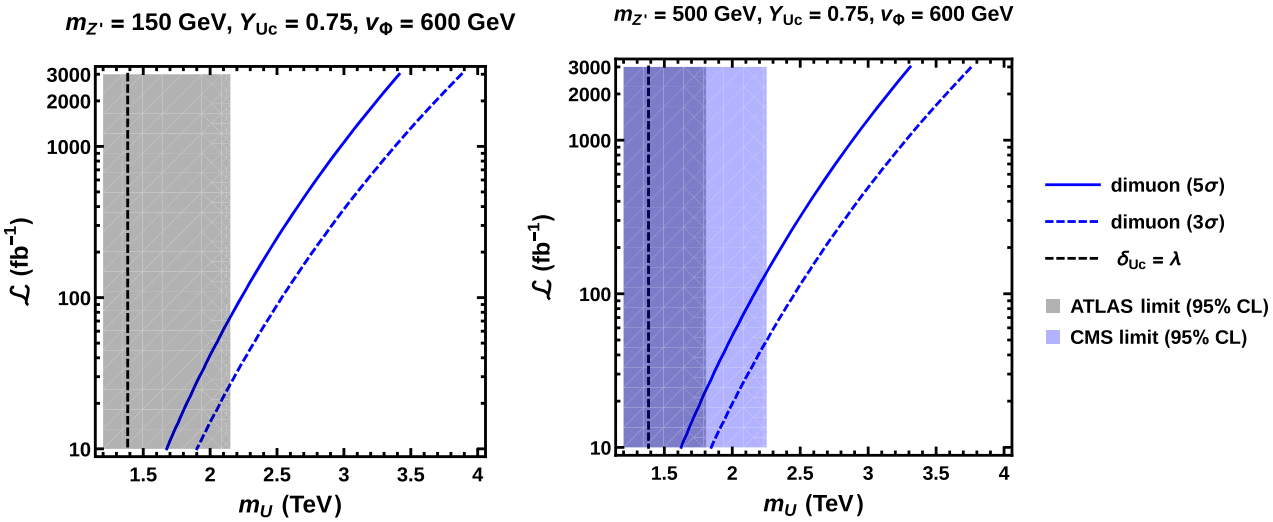

FIG. 11. Same as Fig. 10 but for the dimuon process, with the gray (semitransparent blue) shaded region showing the 95% C.L. exclusion by ATLAS's dimuon resonance search [44] (CMS [45]).

background events. With these results, we plot in the right panel of Fig. 9 the discovery reach for $m_{Z'} = 500$ GeV. The qualitative features are similar to the $m_{Z'} = 150$ GeV case, but the ATLAS constraint is now weaker than the CMS [45] 95% C.L. limit on the dimuon resonance search, as illustrated by the gray shaded region being overlaid by the semitransparent blue shaded region.

Fixing the Yukawa couplings, we can see the *indirect* discovery reach for the vector-like quark mass scale m_U. For illustration, we take a hierarchical pattern of the Yukawa couplings $Y_{Ut} = 1.5$ and $Y_{Uc} = 0.75$ with $v_\Phi = 600$ GeV. In Fig. 10, integrated luminosities required for the discovery of the tZ' process are shown by red solid lines as a function of m_U for $m_{Z'} = 150$ GeV (left) and 500 GeV (right). The red dashed lines are for the 3σ reaches. The vertical dotted lines mark the minimum value of m_U satisfying the small mixing condition $|\delta_{Ut}| \leq \lambda$. With 3000 fb^{-1} data, the discovery of $m_U \simeq 3$ TeV is possible for both $m_{Z'}$ cases.

Similar plots for the dimuon process are given in Fig. 11 for $m_{Z'} = 150$ GeV (left) and 500 GeV (right). The gray (semitransparent blue) shaded region shows the 95% C.L. exclusion from ATLAS's dimuon resonance search [44] (CMS [45]), as in Fig. 9. With 3000 fb^{-1} data, discovery is possible for $m_U \gtrsim 3$ TeV in both $m_{Z'}$ cases. The dimuon resonance search limits increase m_U, such that discovery is possible for the $m_{Z'} = 150(500)$ GeV case after $\sim 80(110)$ fb^{-1} data is accumulated at the 14 TeV LHC, while 3σ evidence can be made with $\sim 30(50)$ fb^{-1} data. This means a discovery could be made with LHC Run 2 data, where experiments can easily change between 13 and 14 TeV collision energies.

Note that the ATLAS and CMS 95% C.L. limits assume a narrow Z' width, while our discovery reach for $m_{Z'} = 500$ GeV is estimated with a rather large width ($\Gamma_{Z'} \simeq 27$ GeV). Note also that CMS gives a stronger limit for $m_{Z'} = 500$ GeV, in part due to the observed limit being better than expected by $\sim 1\sigma$ [45], while our discovery reach was estimated with the inclusion of ATLAS-based detector effects. We have not taken into account systematic uncertainties and backgrounds associated with nonprompt leptons. These would lead to uncertainties in the integrated luminosity for discovery quoted above.

C. Sensitivity of the LH tcZ' coupling motivated by P_5' and R_K anomalies

So far we concentrated on the RH tcZ' coupling, which is inspired by (but not directly linked to) the P_5' and R_K anomalies. Let us now discuss the LH tcZ' coupling that is directly linked to these anomalies.

The LH tcZ' and bsZ' couplings are related by the SU(2)$_L$ relation of Eq. (4): $g^L_{ct} \simeq V_{cs}V^*_{tb}g^L_{sb} + V_{cb}V^*_{tb}g^L_{bb} \sim g^L_{sb} + \lambda^2 g^L_{bb}$, where CKM-suppressed terms are neglected except for the g^L_{bb} term. Using Eq. (7), one can express the first term as $g^L_{sb} = m_{Z'} v_\Phi \Delta C^\mu_9$. The upper and lower limits for v_Φ in Eq. (12) then lead to

$$0.7 \times 10^{-4} \left(\frac{m_{Z'}}{150\ \text{GeV}}\right)\left(\frac{|\Delta C^\mu_9|}{(34\ \text{TeV})^{-2}}\right) \lesssim |g^L_{sb}| \lesssim 0.7 \times 10^{-3}\left(\frac{m_{Z'}}{150\ \text{GeV}}\right). \quad (21)$$

Here, the best-fit value of $\Delta C^\mu_9 \simeq -(34\ \text{TeV})^{-2}$ from a recent global analysis [52] is used in the lower limit, while its dependence is canceled out in the upper limit. The latter is set by the B_s mixing constraint with the Z' effect allowed within 15%. The g^L_{bb} term can be as large as the g^L_{sb} term

if the Yukawa couplings are hierarchical, such that $|g^L_{bb}/g^L_{sb}| = |Y_{Qb}/Y_{Qs}| \sim \lambda^{-2}$, which was indeed advocated in Ref. [17] as a viable solution for the P'_5 anomaly. However, the two terms have opposite sign because $\Delta C^\mu_9 < 0$ implies a negative g^L_{sb}, while g^L_{bb} is positive by definition [see Eq. (6)]. Hence a large g^L_{bb} tends to suppress g^L_{ct}.

We thus conclude that $|g^L_{ct}|$ cannot be larger than $|g^L_{sb}|$. The latter is constrained by Eq. (21). We then obtain the upper limits on the LH tcZ' coupling:

$$|g^L_{ct}|_{\max} \sim \begin{cases} 1\times 10^{-3} & (m_{Z'} = 150\ \text{GeV}), \\ 2\times 10^{-3} & (m_{Z'} = 500\ \text{GeV}), \\ 3\times 10^{-3} & (m_{Z'} = 700\ \text{GeV}). \end{cases} \quad (22)$$

If we set $g^R_{ct} = 0$, we can directly apply the discovery reach of Fig. 8 (left) to the LH coupling g^L_{ct}. We find that, for the P'_5 and R_K motivated case, the maximally allowed values of $|g^L_{ct}|$ are beyond (i.e., smaller than) the discovery reach with 3000 fb^{-1} data, by a factor of 5–10. One cannot even attain 3σ evidence for the $|g^L_{ct}|$ values given in Eq. (22).

We remark that we have estimated the signal tZ' events at LO and have not taken into account QCD corrections, which may enhance the number of signal events. Moreover, the discovery reach might be improved by combining ATLAS and CMS data.

We note in passing that the LH ccZ' coupling is also related to the LH bsZ' coupling, but in a more complicated way: $g^L_{cc} \simeq 2\mathrm{Re}(V_{cs}V^*_{cb}g^L_{sb}) + |V_{cs}|^2 g^L_{ss} + |V_{cb}|^2 g^L_{bb}$, where terms containing the d quark are neglected with the choice of $Y_{Qd} \simeq 0$ for the K and B_d meson mixing constraints. Choosing different Yukawa coupling hierarchies with $m_{Z'} = 150$ GeV, we find the following upper limits on $|g^L_{cc}|$ from the B_s mixing constraint on v_Φ and the small mixing conditions $|\delta_{Qq}| \le \lambda$ [$q = s, c, b, t$, defined as in Eq. (13)]: $|g^L_{cc}| \lesssim 6\times 10^{-4}$ for $Y_{Qb} = 1$, $Y_{Qs} = -1$, and $m_Q = 24$ TeV; $|g^L_{cc}| \lesssim 3\times 10^{-7}$ for $Y_{Qb} = 1$, $Y_{Qs} = -\lambda^2$, and $m_Q = 5.4$ TeV; $|g^L_{cc}| \lesssim 4\times 10^{-3}$ for $Y_{Qb} = \lambda^2$, $Y_{Qs} = -1$, and $m_Q = 5.4$ TeV, where the values for m_Q are chosen such that the best-fit value of $\Delta C^\mu_9 \simeq -(34\ \text{TeV})^{-2}$ is realized. From the right panel of Fig. 8, we read the discovery reach of the dimuon process as $|g^L_{cc}| \gtrsim 2.3\times 10^{-3}$ for $m_{Z'} = 150$ GeV with 3000 fb^{-1} data. Interestingly, the third case with a skewed Yukawa hierarchy $|Y_{Qb}/Y_{Qs}| = \lambda^2$ could be discovered, as long as $v_\Phi \gtrsim 1$ TeV.

V. SUMMARY AND DISCUSSION

The P'_5 and R_K anomalies in $B \to K^{(*)}$ transitions may indicate the existence of a new Z' boson with FCNC couplings. In this paper, we studied the LHC signatures of the RH tcZ' coupling (g^R_{ct}) that is inspired by (but not directly linked to) the $B \to K^{(*)}$ anomalies. We first examined the tcZ'-induced process $cg \to tZ' \to b\nu_\ell \ell^+ \mu^+ \mu^-$ (tZ' process) and its conjugate process ($\bar{t}Z'$ process) at the 14 TeV LHC within the effective theory framework. We then discussed the implications in a specific Z' model, namely, the gauged $L_\mu - L_\tau$ model of Ref. [17]. In this model, the RH tcZ' coupling is induced by mixings of the SU(2)$_L$-singlet vector-like quark U with the top and charm quarks, which also induce the flavor-conserving ccZ' coupling. We thus also considered the $c\bar{c} \to Z' \to \mu^+\mu^-$ (dimuon process) at the LHC. We performed a collider study taking into account detector effects and major SM background processes.

We found that the $\bar{t}Z'$ process has a better chance for discovery than the tZ' process because of smaller backgrounds, and the combination of the two processes (which we also call the tZ' process collectively) can further enhance discovery potential. The tZ' process can be discovered with 3000 fb^{-1} data for a Z' mass in the range 150–700 GeV, with $|g^R_{ct}| = \mathcal{O}(0.01)$ and $\mathcal{B}(Z' \to \mu^+\mu^-) = 1/3$, e.g., $|g^R_{ct}| \gtrsim 0.0047$ (0.013) for $m_{Z'} = 150(500)$ GeV. Reinterpreted within the gauged $L_\mu - L_\tau$ model, these results imply that one can discover the Z' if the mixing parameters of the vector-like quark U with the top and charm quarks, δ_{Ut} and δ_{Uc}, are $\mathcal{O}(0.1)$ and the VEV of the exotic Higgs is not too large, i.e., $v_\Phi \lesssim 2$ TeV. In the model, the tZ' and dimuon processes are correlated, with the dimuon process having better discovery potential if $|\delta_{Ut}| \sim |\delta_{Uc}|$, starting with LHC Run 2 data. But if the mixings are hierarchical, such that $|\delta_{Uc}/\delta_{Ut}| \lesssim 0.4$, the tZ' process would have better discovery potential. However, g^R_{ct} tends to be suppressed in this case, and discovery is not possible at the HL-LHC if $|\delta_{Uc}/\delta_{Ut}| \lesssim \lambda \simeq 0.23$ with $|\delta_{Ut}| \le \lambda$ for v_Φ values allowed by the neutrino trident production. We illustrated the discovery zones in the model by imposing the existing ATLAS and CMS dimuon resonance search constraints, and showed that there exist interesting parameter regions where both the tZ' and dimuon processes can be discovered. If this is the case, the simultaneous measurement of the two processes could uncover the flavor structure of the model.

We also discussed the sensitivity for the LH tcZ' coupling g^L_{ct} that is directly linked to the $B \to K^{(*)}$ anomalies. We first identified the range of the LH bsZ' coupling g^L_{sb} favored by the $b \to s\ell^+\ell^-$ transition data, and then obtained the upper limits on $|g^L_{ct}|$ using SU(2)$_L$ symmetry. We found that the $|g^L_{ct}|$ values implied by the $B \to K^{(*)}$ anomalies are beyond the discovery reach of the tZ' process at the HL-LHC. However, the sensitivity might be improved by the inclusion of QCD corrections to the signal cross section, and/or by combining ATLAS and CMS data.

The gauged $L_\mu - L_\tau$ model further implies flavor-conserving ttZ' couplings, which lead to the $pp \to t\bar{t}Z'$ production process at the LHC. This process may provide

not only another discovery channel of the Z', but also useful information on the flavor structure of the model. In particular, the three production modes (namely, tZ', dimuon, and $t\bar{t}Z'$ processes) can be correlated by the dependence on the two Yukawa couplings Y_{Ut} and Y_{Uc}. We note that the ccZ' couplings can be also probed through the $cg \to cZ'$ process, if one has efficient charm tagging. These will be studied elsewhere.

In this paper, we focused on collider signatures of the Z' couplings to the top and charm quarks, but discovery of the Z' may also come from the couplings to the down-type quark sector. In particular, the gauged $L_\mu - L_\tau$ model predicts a nonzero LH bbZ' coupling g^L_{bb} if the LH bsZ' coupling exists. The bbZ' coupling induces the process $b\bar{b} \to Z' \to \mu^+\mu^-$ and can be searched in a similar way as the ccZ' coupling at the LHC. Taking for illustration $m_{Z'} = 200$ GeV, $v_\Phi = 1.5$ TeV, $Y_{Qb} = 1$, $Y_{Qs} = -\lambda^2$, and $m_Q = 24$ TeV, giving $\Delta C^\mu_9 = -(34\ \text{TeV})^{-2}$ for the $B \to K^{(*)}$ anomalies, we find $g^L_{bb} \simeq 5 \times 10^{-3}$ and an induced Z' production cross section $\sigma(pp \to Z') \simeq 30$ fb at the 14 TeV LHC using MadGraph. Multiplying $\mathcal{B}(Z' \to \mu^+\mu^-) \simeq 1/3$ and assuming similar cuts and detector effects as in the ccZ'-induced dimuon process, we obtain the cross section $\sigma(pp \to Z' \to \mu^+\mu^-) \simeq 4$ fb with the event selection cuts. Utilizing the background cross sections for the dimuon process in Table IV, we then find that such a Z' can be discovered with $\sim$1000 fb^{-1} integrated luminosity. The $b\bar{b} \to Z'$ production process has also been studied in other Z' models constructed for the $B \to K^{(*)}$ anomalies [53,54].

We emphasize that the RH tcZ' coupling cannot be constrained well by B and K physics, but is on similar footing as the current $B \to K^{(*)}$ anomalies. In particular, the coupling may exist even if the P'_5 and R_K anomalies evaporate in the future. Hence, it is important to explore the RH tcZ' coupling regardless of the fate of the $B \to K^{(*)}$ anomalies, with the potential of discovering a new Z' gauge boson as a dimuon resonance with weaker and FCNC quark couplings. Our study therefore illustrates the unique role of *top* physics in the flavor program. If a discovery is made at the LHC, one would then need to probe the handedness of the coupling via angular distributions, while a $c\bar{c} \to Z'$ discovery (and maybe also $cg \to cZ'$ and $t\bar{t}Z'$) would provide complementary information, opening up a rich program.

ACKNOWLEDGMENTS

We thank Y. Chao for discussions. W. S. H. is supported by grants MOST 104-2112-M-002-017-MY2, MOST 105-2112-M-002-018, and NTU 105R8965. M. K. is supported by NTU-105R104022 and NTU-G029927. T. M. is supported by MOST-104-2112-M-002-017-MY2.

[1] R. Aaij *et al.* (LHCb Collaboration), Phys. Rev. Lett. **111**, 191801 (2013).
[2] R. Aaij *et al.* (LHCb Collaboration), J. High Energy Phys. 02 (2016) 104.
[3] R. Aaij *et al.* (LHCb Collaboration), Phys. Rev. Lett. **113**, 151601 (2014).
[4] S. Wehle *et al.* (Belle Collaboration), Phys. Rev. Lett. **118**, 111801 (2017).
[5] S. Descotes-Genon, J. Matias, and J. Virto, Phys. Rev. D **88**, 074002 (2013).
[6] W. Altmannshofer and D. M. Straub, Eur. Phys. J. C **73**, 2646 (2013).
[7] F. Beaujean, C. Bobeth, and D. van Dyk, Eur. Phys. J. C **74**, 2897 (2014); **74**, 3179(E) (2014).
[8] R. R. Horgan, Z. Liu, S. Meinel, and M. Wingate, Phys. Rev. Lett. **112**, 212003 (2014).
[9] T. Hurth and F. Mahmoudi, J. High Energy Phys. 04 (2014) 097.
[10] R. Alonso, B. Grinstein, and J. Martin Camalich, Phys. Rev. Lett. **113**, 241802 (2014).
[11] G. Hiller and M. Schmaltz, Phys. Rev. D **90**, 054014 (2014).
[12] D. Ghosh, M. Nardecchia, and S. A. Renner, J. High Energy Phys. 12 (2014) 131.
[13] T. Hurth, F. Mahmoudi, and S. Neshatpour, J. High Energy Phys. 12 (2014) 053.
[14] W. Altmannshofer and D. M. Straub, Eur. Phys. J. C **75**, 382 (2015).
[15] X. G. He, G. C. Joshi, H. Lew, and R. R. Volkas, Phys. Rev. D **43**, R22 (1991).
[16] R. Foot, Mod. Phys. Lett. A **06**, 527 (1991).
[17] W. Altmannshofer, S. Gori, M. Pospelov, and I. Yavin, Phys. Rev. D **89**, 095033 (2014).
[18] K. Harigaya, T. Igari, M. M. Nojiri, M. Takeuchi, and K. Tobe, J. High Energy Phys. 03 (2014) 105.
[19] W. Altmannshofer, S. Gori, M. Pospelov, and I. Yavin, Phys. Rev. Lett. **113**, 091801 (2014).
[20] F. del Aguila, M. Chala, J. Santiago, and Y. Yamamoto, J. High Energy Phys. 03 (2015) 059.
[21] F. Elahi and A. Martin, Phys. Rev. D **93**, 015022 (2016).
[22] K. Fuyuto, W.-S. Hou, and M. Kohda, Phys. Rev. D **93**, 054021 (2016).
[23] A. Arhrib, K. Cheung, C.-W. Chiang, and T.-C. Yuan, Phys. Rev. D **73**, 075015 (2006).

[24] O. Cakir, I. T. Cakir, A. Senol, and A. T. Tasci, Eur. Phys. J. C **70**, 295 (2010).
[25] J. I. Aranda, F. Ramirez-Zavaleta, J. J. Toscano, and E. S. Tututi, J. Phys. G **38**, 045006 (2011).
[26] S. K. Gupta and G. Valencia, Phys. Rev. D **82**, 035017 (2010).
[27] M. I. Gresham, I. W. Kim, and K. M. Zurek, Phys. Rev. D **84**, 034025 (2011).
[28] J. N. Ng and P. T. Winslow, J. High Energy Phys. 02 (2012) 140.
[29] A. M. Sirunyan *et al.* (CMS Collaboration), arXiv: 1702.01404.
[30] S. R. Mishra *et al.* (CCFR Collaboration), Phys. Rev. Lett. **66**, 3117 (1991).
[31] S. Schael *et al.* (ALEPH, DELPHI, L3, OPAL, and SLD Collaborations, LEP Electroweak Working Group, SLD Electroweak Group, and Heavy Flavour Group), Phys. Rep. **427**, 257 (2006).
[32] A. Crivellin, G. D'Ambrosio, and J. Heeck, Phys. Rev. Lett. **114**, 151801 (2015).
[33] J. Campbell, R. K. Ellis, and R. Röntsch, Phys. Rev. D **87**, 114006 (2013).
[34] J. M. Campbell and R. K. Ellis, J. High Energy Phys. 07 (2012) 052.
[35] ATLAS Collaboration, Report No. ATLAS-CONF-2014-058.
[36] J. Alwall, R. Frederix, S. Frixione, V. Hirschi, F. Maltoni, O. Mattelaer, H.-S. Shao, T. Stelzer, P. Torrielli, and M. Zaro, J. High Energy Phys. 07 (2014) 079.
[37] T. Sjöstrand, L. Lönnblad, S. Mrenna, and P. Z. Skands, arXiv:hep-ph/0308153.
[38] J. Alwall *et al.*, Eur. Phys. J. C **53**, 473 (2008).
[39] J. de Favereau, C. Delaere, P. Demin, A. Giammanco, V. Lemaître, A. Mertens, and M. Selvaggi (DELPHES 3 Collaboration), J. High Energy Phys. 02 (2014) 057.
[40] A. Alloul, N. D. Christensen, C. Degrande, C. Duhr, and B. Fuks, Comput. Phys. Commun. **185**, 2250 (2014).
[41] J. Pumplin, D. R. Stump, J. Huston, H.-L. Lai, P. M. Nadolsky, and W.-K. Tung, J. High Energy Phys. 07 (2002) 012.
[42] M. Grazzini, S. Kallweit, D. Rathlev, and M. Wiesemann, Phys. Lett. B **761**, 179 (2016).
[43] G. Cowan, K. Cranmer, E. Gross, and O. Vitells, Eur. Phys. J. C **71**, 1 (2011); **73**, 2501(E) (2013).
[44] ATLAS Collaboration, Report No. ATLAS-CONF-2016-045.
[45] CMS Collaboration, Report No. CMS-PAS-EXO-16-031.
[46] CMS Collaboration, Report No. CMS-PAS-EXO-15-005.
[47] Y. Li and F. Petriello, Phys. Rev. D **86**, 094034 (2012).
[48] ATLAS and CMS Collaborations recommended predictions for top-quark-pair cross sections: https://twiki.cern.ch/twiki/bin/view/LHCPhysics/TtbarNNLO.
[49] N. Kidonakis, Phys. Rev. D **82**, 054018 (2010).
[50] T. Gehrmann, M. Grazzini, S. Kallweit, P. Maierhöfer, A. von Manteuffel, S. Pozzorini, D. Rathlev, and L. Tancredi, Phys. Rev. Lett. **113**, 212001 (2014).
[51] F. Cascioli, T. Gehrmann, M. Grazzini, S. Kallweit, P. Maierhöfer, A. von Manteuffel, S. Pozzorini, D. Rathlev, L. Tancredi, and E. Weihs, Phys. Lett. B **735**, 311 (2014).
[52] S. Descotes-Genon, L. Hofer, J. Matias, and J. Virto, J. High Energy Phys. 06 (2016) 092.
[53] S. M. Boucenna, A. Celis, J. Fuentes-Martin, A. Vicente, and J. Virto, J. High Energy Phys. 12 (2016) 059.
[54] P. Ko, T. Nomura, and H. Okada, arXiv:1701.05788.